

Quantum channel correction outperforming direct transmission

Author

Slussarenko, S, Weston, MM, Shalm, LK, Verma, VB, Nam, SW, Kocsis, S, Ralph, TC, Pryde, GJ

Published

2022

Journal Title

Nature Communications

Version

Version of Record (VoR)

DOI

[10.1038/s41467-022-29376-4](https://doi.org/10.1038/s41467-022-29376-4)

Rights statement

© The Author(s) 2022. This article is licensed under a Creative Commons Attribution 4.0 International License, which permits use, sharing, adaptation, distribution and reproduction in any medium or format, as long as you give appropriate credit to the original author(s) and the source, provide a link to the Creative Commons license, and indicate if changes were made.




Downloaded from

<http://hdl.handle.net/10072/414211>

Griffith Research Online

<https://research-repository.griffith.edu.au>

Quantum channel correction outperforming direct transmission

Sergei Slussarenko¹  [✉], Morgan M. Weston¹, Lynden K. Shalm², Varun B. Verma², Sae-Woo Nam², Sacha Kocsis^{1,4}, Timothy C. Ralph³  [✉] & Geoff J. Pryde¹  [✉]

Long-distance optical quantum channels are necessarily lossy, leading to errors in transmitted quantum information, entanglement degradation and, ultimately, poor protocol performance. Quantum states carrying information in the channel can be probabilistically amplified to compensate for loss, but are destroyed when amplification fails. Quantum correction of the channel itself is therefore required, but break-even performance—where arbitrary states can be better transmitted through a corrected channel than an uncorrected one—has so far remained out of reach. Here we perform distillation by heralded amplification to improve a noisy entanglement channel. We subsequently employ entanglement swapping to demonstrate that arbitrary quantum information transmission is unconditionally improved—i.e., without relying on postselection or post-processing of data—compared to the uncorrected channel. In this way, it represents realization of a genuine quantum relay. Our channel correction for single-mode quantum states will find use in quantum repeater, communication and metrology applications.

¹Centre for Quantum Dynamics and Centre for Quantum Computation and Communication Technology, Griffith University, Brisbane, QLD, Australia. ²National Institute of Standards and Technology, Boulder, CO, USA. ³Centre for Quantum Computation and Communication Technology, School of Mathematics and Physics, University of Queensland, St Lucia, QLD, Australia. ⁴Present address: Centre for Quantum Computation and Communication Technology, The University of New South Wales, Sydney, NSW, Australia. ✉email: s.slussarenko@griffith.edu.au; ralph@physics.uq.edu.au; g.pryde@griffith.edu.au

Loss-induced noise, e.g., from scattering and diffraction, is inevitable in long-distance information transfer. Although some communication schemes permit postprocessing of measurement results to discard vacuum or noise, high-demand applications such as device-independent protocols¹, distributed quantum computing^{2,3}, or quantum metrology schemes⁴ cannot rely on postselection. Such applications require genuine entanglement distillation schemes to overcome the effects of loss. Therefore, fully heralded protocols that can demonstrably show an advantage in transmitting states over a noise-reduced entanglement channel are critically important. This is the quantum communication equivalent of surpassing the break-even point for quantum error correction⁵.

Photon linear loss reduces the amplitude of the creation operator associated with a particular mode (channel) according to a linear transformation, and adds noise by mixing in one or more other optical modes in the process. This process is gaussian, mapping one gaussian distribution onto another. Loss-induced noise affects any type of optical encoding. It provides a particular challenge for coherent and squeezed states, as it has been proven that it is impossible to correct gaussian noise on gaussian states using only gaussian operations⁶.

Techniques for addressing loss-induced noise broadly include entanglement-swapping-based quantum nondemolition style measurements^{7–10} and their extensions^{11–14}, distillation techniques based on noiseless linear amplification^{15–18}, and photonic qubit precertification¹⁹. Among these, schemes based on noiseless linear amplification (or heralded amplification, HA) have shown great potential in amplifying single-mode¹⁵ or two-mode^{20,21} qubits, correcting for the effects of loss on entangled states^{15,18,22}, and in conditionally exceeding quantum cloning bounds²³.

In the absence of error correcting codes, noise reduction in quantum mechanics is necessarily probabilistic and one needs to consider how this affects the noise mitigation process. Broadly, noise reduction or correction can be grouped into three categories: postselection, where final detection of the (probabilistically) corrected state identifies whether correction was successful; heralded state correction, where an independent signal flags (or heralds) noise reduction on the state without need for postselection but where the state is destroyed upon failure; and heralded channel correction, where successful heralding prepares a channel that can be used to transmit a state, and one can refrain from sending the state if channel noise reduction fails. Each of these tasks is more challenging than the previous.

Here, we experimentally implement heralded channel correction using HA¹⁵, use it to distribute entanglement via entanglement swapping⁷ and demonstrate reduced loss-induced errors in a quantum channel²⁴. Our scheme thus demonstrates the core task of a quantum relay in distributing quantum information over a channel affected by loss.

Results

Theory. From an information perspective, the channel is represented by an entangled subsystem of quantum optical modes. Such entanglement, once corrected for loss, can be used to implement a quantum teleportation scheme to transfer quantum information across the channel. The specific type of mode entanglement we generate for this channel is obtained by splitting a single photon between two modes. This single-rail encoding²⁵ is of current interest^{26,27} due to its applications in twin-field quantum key distribution protocols²⁸ and recently demonstrated techniques for converting between single-rail and dual-rail encoding²⁹.

The theoretical concept is shown in Fig. 1 and explained using the language of single-mode qubits, i.e., superpositions of the vacuum and single-photon state in a single optical mode. First consider Fig. 1a–c. The aim is to transmit such a qubit $|\psi_{\text{in}}\rangle = \alpha|0_e\rangle + \beta|1_e\rangle$, initially encoded in mode “e”, as per Fig. 1a. Transmission of “e” through a lossy channel degrades it to

$$\rho_{\text{out}} = |\beta|^2(1 - T)|0\rangle\langle 0| + (\alpha|0\rangle + \sqrt{T}\beta|1\rangle)(\alpha^*\langle 0| + \sqrt{T}\beta^*\langle 1|), \quad (1)$$

where the transmission T can also be written as $1 - L$ with L being the loss. It has been shown that postselection-based filtering can reduce the noise on states of this general kind³⁰, but this is useful for a limited range of applications. Alternatively, a heralded amplifier (Fig. 1b), applied after the loss, changes the degraded state according to

$$\rho_{\text{HA}} \rightarrow (1 - P_{\text{amp}})|0\rangle\langle 0| \otimes \Pi_{\text{namp}} + P_{\text{amp}}\rho_{\text{amp}} \otimes \Pi_{\text{amp}}, \quad (2)$$

where P_{amp} is the probability of success of the amplification and Π_{amp} (Π_{namp}) is the projector onto the subspace of where the heralding signal was (not) received. The amplified state ρ_{amp} is given by

$$\rho_{\text{amp}} = \frac{|\beta|^2(1 - T)|0\rangle\langle 0| + (\alpha|0\rangle + g\sqrt{T}\beta|1\rangle)(\alpha^*\langle 0| + g\sqrt{T}\beta^*\langle 1|)}{1 + T|\beta|^2(g^2 - 1)}, \quad (3)$$

where $g \geq 1$ is the (amplitude) amplification gain. If $g = 1$, the HA acts as a single-mode teleportation stage without amplification.

Although the heralded amplifier can be used to mitigate the effect of loss on the quantum state in the sense that the average fidelity of Eq. (3) with the initial state exceeds that of Eq. (1), the fidelity increase is strictly limited (see Supplementary Section 2). In addition, by itself it is not sufficient to correct for errors in a quantum channel, as information will still be lost in cases when amplification did not succeed. An alternative approach is to use a two-mode entangled state

$$|\psi_{\text{fe}}\rangle = \frac{|1_f 0_e\rangle + |0_f 1_e\rangle}{\sqrt{2}}, \quad (4)$$

as in Fig. 1c. Such a state represents an entanglement-based channel as it can act as a resource for single-mode teleportation. Once the HA has successfully corrected the mode “e” from the effects of loss, the other mode “f” is used to implement a quantum teleportation scheme to teleport the desired quantum information $|\psi_{\text{in}}\rangle$, encoded in a qubit in mode “g”, to the output mode “v” of the HA. Effectively we have a deterministic, error corrected channel. In the limit of high HA gain and using biased entanglement we can in principle approach an error free channel for any finite level of loss^{17,22,31} (see Supplementary Section 2).

Protocol. An alternative but equally interesting scenario—shown in Fig. 1d—is to consider the transmission of half of a two-mode entangled state (rather than $|\psi_{\text{in}}\rangle$) through the channel. This is the situation we implement in this work. The outcome of such a scheme is an entangled state distributed between modes “h” and “v”, that can be used for further information tasks, in principle. Characterizing the success of the channel correction consists of comparing the amount of entanglement between modes “h” and “v” in the case of Fig. 1d to the amount of entanglement in case of direct transmission of a mode of an entangled qubit through loss. We note that if the channel is capable of teleporting entanglement, it can also teleport arbitrary quantum states and, hence entanglement swapping tests the quality with which all possible

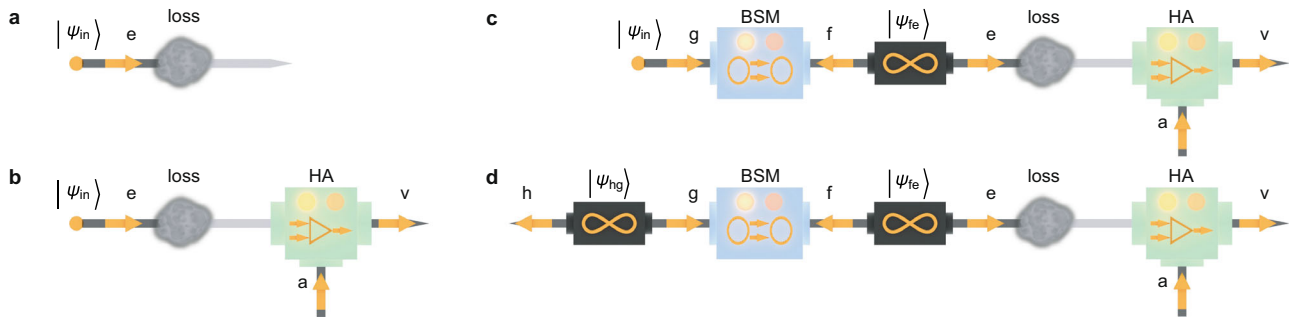


Fig. 1 Conceptual representations of quantum state transmission through a lossy channel, with and without correction. **a** A quantum state, here a qubit encoded in a single mode “e”, is transmitted through a lossy channel, which degrades the state quality. **b** After the loss, the noisy state can be corrected using a heralded amplifier (HA). Mode “a” carries the ancilla photon that powers the HA. The operation of HA has an independent success signal, so postselection is not required. However, HA failure destroys the state. **c** By adding a mode-entangled state $|\psi_{fe}\rangle$, success of the HA heralds a noise-corrected quantum channel. This can be used upon success by teleporting a qubit in mode “g” onto mode “v” via a Bell state measurement (BSM) between “g” and “f”. **d** Instead of transmitting a qubit $|\psi_{in}\rangle$ through the lossy or corrected channel, it is possible to transmit half of an entangled state, leading to distributed entanglement through a heralded corrected channel in the last case.

input states of the relevant Hilbert space can be teleported through the channel.

The single-mode heralded amplification (HA) and entanglement swapping (ES) stages can be implemented with the generalized quantum scissors^{15,32}. In this approach, the input state is interfered non-classically on a beam splitter with one of the modes (mode “a” in this example) of a resource state $|\psi_{av}\rangle = \sqrt{\eta}|1_a0_v\rangle + \sqrt{1-\eta}|0_a1_v\rangle$. The success of the operation is conditioned on getting one and only one detection event in one of the two auxiliary detectors. The difference between entanglement swapping and HA operations is the setting $\eta = 1/2$ or $\eta < 1/2$, respectively, with the nominal intensity gain given by $g^2 = (1 - \eta)/\eta$ in an ideal case of perfect interference, unit delivery efficiency of $|\psi_{av}\rangle$ and absence of noise.

For a small state which exists in the $\{0, 1\}$ photon number subspace, a one-to-one mapping exists between pairs of entangled orthogonal spatial modes and a photon polarization qubit:

$$|\psi_{in}\rangle = \alpha|1_H0_V\rangle + \beta|0_H1_V\rangle = \alpha|H\rangle + \beta|V\rangle, \quad (5)$$

where H and V represent horizontal and vertical polarizations, respectively. For such encoding, mode manipulation is implemented via polarizing beam splitters (PBS) and half- and quarter-wave plates (HWP and QWP), instead of beam splitters.

Experiment. Our experimental realization of the error-correction scheme of Fig. 1d is shown in Fig. 2. We use two photon-pair sources, based on group velocity matched spontaneous parametric downconversion (GVM SPDC), to generate the photons required for the scheme (see Methods for details). One photon-pair source was used to prepare the resource state $|\psi_{fe}\rangle = (|H_f\rangle + |V_e\rangle)/\sqrt{2}$ and the mode-entangled state for entanglement swapping $|\psi_{hg}\rangle = (|H_h\rangle + |V_g\rangle)/\sqrt{2}$. Another source was used to prepare a heralded single photon state $|\psi_{av}\rangle$ as the resource that powers the HA.

The task of demonstrating improved entanglement when transmitting over a heralded corrected channel has stringent technological requirements. High-heralding-efficiency, low noise photon sources, high quality quantum interference, and high-efficiency detectors are necessary in order to complete a 4-photon protocol in such a way that demonstrates improvement over a simple transmission of a single photon, even taking into account the loss. We describe the substance of these requirements, and our means for satisfying them—high-efficiency GVM SPDC sources that directly produce spectrally pure photon pairs,

together with high-efficiency superconducting nanowire photon detectors—in the Methods.

In the $\{|0\rangle, |1\rangle\}$ photon number subspace the density matrix of a two-mode entangled state can be represented as $\rho = p_{00}|00\rangle\langle 00| + p_{01}|01\rangle\langle 01| + p_{10}|10\rangle\langle 10| + d|01\rangle\langle 10| + d^*|10\rangle\langle 01| + p_{11}|11\rangle\langle 11|$. We assume zero coherence between vacuum, single-photon, and two-photon components of the state. We use concurrence³³ to characterize the entanglement it carries, which in this case is given by

$$C = 2\text{Max}[|d| - \sqrt{\rho_{00}\rho_{11}}, 0]. \quad (6)$$

Its explicit dependence on the vacuum ρ_{00} and high-order ρ_{11} contributions highlights the detrimental effect of loss and higher-order photon emission noise on our scheme. We measure these quantities and $|d|$ by directly measuring the probabilities of detecting vacuum, one- and two-photon component, together with performing a quantum state tomography on output modes of the transmission.

To demonstrate the advantage of our channel error-correction scheme, we first measured the amount of entanglement carried by the state $|\psi_{fe}\rangle$ transmitted through the polarization-dependent loss (as in Fig. 2d). We then compared the result to the amount of entanglement of the same entangled state distributed via the channel error-correction scheme, by measuring the concurrence between modes “h” and “v”, heralded by the corresponding click pattern of the detectors in the HA and ES stages (as in Figs. 1d and 2b).

Our experimental results, together with theoretical predictions, are shown in Fig. 3 for three different values of added loss on mode “e”. Our experimental data matches theoretical predictions, derived from a quantum circuit model that includes measured efficiencies and higher order emission from the sources but with no free fit parameters. We attribute the slight reduction of the experimentally observed concurrence to the non-perfect HOM interference at the HA stage, which was not taken into account in the theoretical model. It is worth noting that maximum observed concurrence in the state transmitted through the error-corrected channel does not correspond to the gain setting that recovers the state to $(|H\rangle + |V\rangle)/\sqrt{2}$, but to a nominal gain setting at which mode “e” is over-amplified, as shown in Fig. 4.

For the comparison in Fig. 3 between the two different channels to be fair, it is important to take into account the channels’ operation rates. Due to the probabilistic nature of SPDC, the probability of generating four photons for the error corrected channel is significantly lower than the probability of

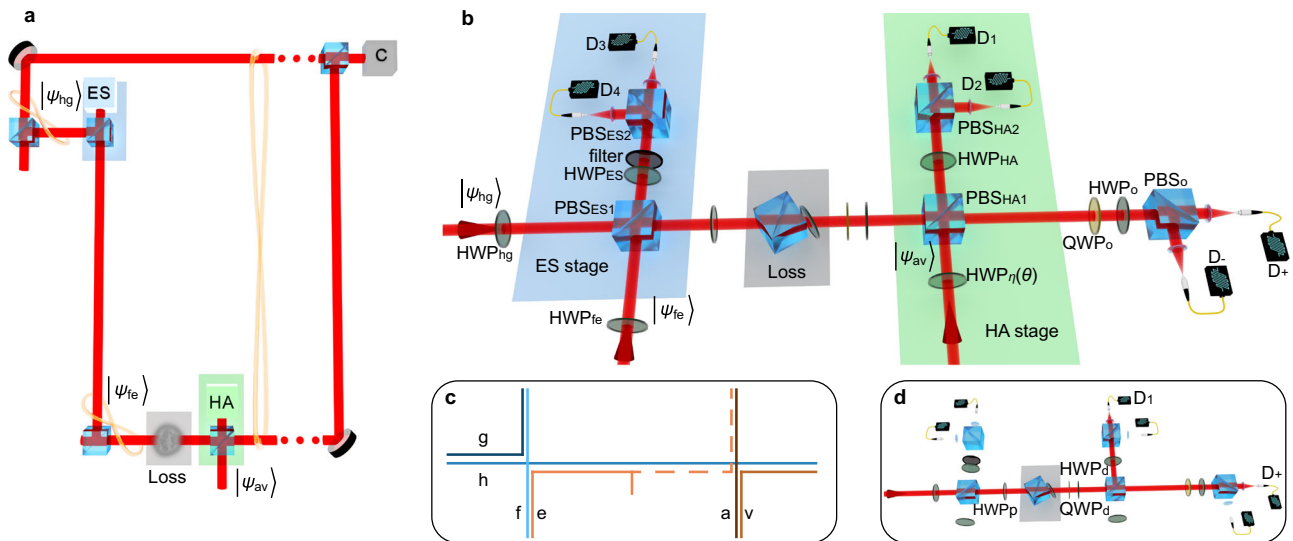


Fig. 2 Concept and layout of the experimental apparatus. **a** Concept of the experiment, which implements the scheme of Fig. 1d. Half of the entangled state $|\psi_{hg}\rangle$ is teleported through a heralded corrected channel. This comprises an entangled source, loss on one mode (the distribution mode), and an HA. This leads to entanglement between modes “h” and “v” that, ideally, is larger than the entanglement between “f” and “e” after “e” goes through the lossy channel. Modes “h” and “v” are then brought together for a joint measurement to determine the concurrence C. **b** Experimental setup for the error-corrected quantum channel. This diagram has a one-to-one mode mapping to part **a**, as shown in subfigure **c**, but some of the modes are now spatially overlaid and distinguished by polarization. Blue and green backgrounds highlight ES and HA stages, respectively. Gray background highlights polarization dependent loss. Optical axes of HWP_{fe} and HWP_{hg}, set at $\pi/8$ with respect to the horizontal axis, prepared $|\psi_{fe}\rangle$ and $|\psi_{hg}\rangle$ states, respectively. Optical modes input to PBS_{HA2} and PBS_{ES2} were mixed by HWP_{HA} and HWP_{ES}, set at $\pi/8$. HWP_{r(θ)}, with optic axis orientated at angle θ , initialized the HA resource state $|\psi_{av}\rangle$, with $\eta = \sin(2\theta)$. HA success was heralded by a single detection event in either superconducting nanowire single photon detector (SNSPD) D₁ or D₂ and ES success was heralded by a single detection event in either D₃ or D₄. Detectors D₊ and D₋, together with QWP_o, HWP_o and PBS_o were used to perform polarization state tomography on the modes “h” and “v”. **c** Mode propagation inside the setup in case of the error-corrected channel. Mode “h” propagates through the setup unaffected by loss or other optical components. **d** Same setup but with single photon input, used to test direct transmission through loss to compare the final concurrences. HWP_p was set to $\pi/8$ in order to prepare $|\psi_{fe}\rangle$. QWP_d, HWP_d and PBS_{HA1}, together with detectors D₊ and D₁ were used to perform polarization tomography of the state after the loss. Note that the ultrahigh-heralding-efficiency photon sources required for this protocol are not shown in the figure—see Methods for details.

generating one photon pair for the direct transmission. This leads to lower raw coincidence counts per second in the former case. For a fair comparison we define the operation rate as the rate of input states prepared and sent through the channel, given successful preparation of the channel. As described in Supplementary Section 3, we find that the operation rate of the error corrected channel is higher or equal to the rate of direct transmission, thus providing us a level playing field for the direct comparison of the concurrences for the two scenarios and showcasing the power of our error-corrected channel scheme.

Discussion

The challenge of overcoming loss in a quantum channel is central for realizing many quantum technologies, including quantum computation and communication. We have demonstrated error-correction of a quantum channel, in a heralded way. Comparing to a much simpler, direct transmission of a single optical mode through loss, our scheme provides unconditional advantage, despite being experimentally more complex. With our best result we have observed up to a factor of $F = 4.1 \pm 0.3$ increase in concurrence over direct transmission, equivalent to an effective improvement in the channel transmission of ≈ 12.9 dB. In principle, it is possible to implement the entanglement swapping operation only after the HA success signal certifies that the channel is ready for transmission—we do not implement that strict time ordering in this experiment. In our experiment verification of the entanglement utilizes lossless transmission of the “h” reference mode from sender to receiver. However, this is done for simplicity and is not fundamental. In the field such

characterization could be achieved by interfering the outputs locally with classical optical phase references (known technically as ‘local oscillators’), followed by appropriate (homodyne) detection. Producing remote, synchronized phase references has been demonstrated in continuous variable and twin-field applications.

Methods

Requirements for experimental advantage. It is challenging to meet the performance requirements of our scheme in the presence of several inevitable experimental imperfections. First, the HA efficiency is limited by the efficiency of $|\psi_{av}\rangle$ delivery and detection³⁴. Moreover, the photons that interfere at the HA stage of our setup are generated by two different photon-pair sources. The use of photons from an independent source for $|\psi_{av}\rangle$ is motivated by the fact that this photon is used on the other side from the loss, which in a field-deployed application would represent a long optical channel, and thus it cannot be generated by the same source as the resource states $|\psi_{fe}\rangle$ and $|\psi_{hg}\rangle$. Quantum (Hong-Ou-Mandel or HOM) interference of photons from independent sources requires photons that are spectrally pure and indistinguishable. The conventional approach is to apply lossy spectral filtering. In this case, the extra loss does not only reduce the efficiency of the HA stage, but also increases the negative effect of high-photon number noise on the error-correction scheme. Such noise appears due to the events when more than one photon pair is generated from the same source at the same time. In our case, this would have reduced HOM interference visibility at the ES and HA stages, leading to false-positive heralding events and directly affecting the final state in terms of the amount of entanglement it carries. HOM interference visibilities and heralding efficiencies provided by photon source technology employed in previous works including Ref. 20 are insufficient to demonstrate the advantage of our scheme without relying on postselection, which was enabled by the high-performance source and detector configuration that we describe next.

Experimental details. Our heralded single-photon sources³⁵ consisted of two 2mm nonlinear periodically poled potassium titanyl phosphate crystal (pp-KTP, poling period 46.20 μm), phase-matched for type-II collinear operation, pumped by

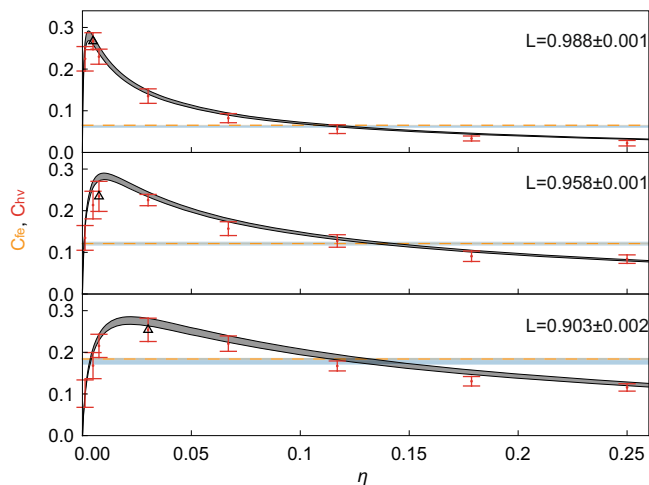


Fig. 3 Concurrence measurements of entanglement distributed over different types of channels for three different values of added loss L on mode “e”. Orange lines and blue shaded areas correspond to the experimentally measured and theoretically predicted concurrence C_{fe} of $|\psi_{fe}\rangle$ state distributed directly through loss. Red dots and gray shaded areas correspond to the experimentally measured and theoretically predicted concurrence C_{hv} of entanglement distributed via the error-corrected quantum channel Fig. 1d, with the same amount of loss and the same input state $|\psi_{fe}\rangle$. Black triangles highlight data points with maximum observed increase in concurrence. The upper and lower bounds for the theoretical predictions correspond to the lowest and highest observed transmissions for each mode inside the experimental setup, respectively. Error bars and shaded areas on orange lines correspond to the experimentally observed statistical uncertainty of ± 1 standard deviation.

a mode-locked Ti:sapphire laser with ≈ 81 MHz repetition rate, 775 nm wavelength and 6 nm full-width at half-maximum (FWHM) bandwidth. SPDC from the pp-KTP crystals produced degenerate photon pairs centered at 1,550 nm wavelength and with ≈ 15 nm FWHM bandwidth. The pump and collection beam waist sizes were set to 170 μ m and 50 μ m, respectively, in order to optimize the output mode matching to an optical single mode fiber. Connecting our sources directly to high-efficiency SNSPDs³⁶, we achieved symmetric heralding efficiencies³⁷ of ≈ 0.8 . In the experimental setup, the observed delivery efficiency of $|\psi_{av}\rangle$, including all the optical losses and non-unit detection efficiency, ranged from 0.635 ± 0.004 to 0.757 ± 0.004 , depending on the particular output path towards detectors D_1, D_2, D_+, D_- . The lower efficiency (compared to the value for source and detectors only) is due to the delivery efficiency which includes non-unit transmission of polarizing beam splitters (PBS) inside the HA and measurement stages and different efficiency of the SNSPDs at different outputs.

The GVM SPDC sources generate photon pairs with high intrinsic spectral purity, providing HOM interference visibility up to 0.84 between photons from independent sources without applying any spectral filtering. This number can be boosted up to almost one by applying mild spectral filtering only on the corresponding herald photons³⁵, leaving interfering photons unfiltered and thus not affected by extra loss. Recent advances in design and engineering of poling of nonlinear crystals were able to provide photon-pair sources that require no filtering at all to achieve almost unit HOM interference visibility between photons from different sources³⁸. Our work did not rely on such poling engineering and we achieved high-visibility interference by applying bandpass filters with ≈ 8 nm FWHM on the herald of $|\psi_{av}\rangle$ and on the photons that propagate inside the ES stage of the setup, as shown in Fig. 2a. No spectral filtering was applied on the photons that interfered at the HA stage. In such configuration, we observe independent (photons from different sources) HOM interference visibility of up to 0.97 ± 0.03 at the HA stage and dependent (photons from the same source) HOM interference visibility of 0.990 ± 0.001 at the ES stage, see Supplementary Figure 1.

The pump power of the sources was set so to achieve pair-per-pulse generation probability of $p \approx 0.00123$, equivalent to a probability of $p^2 \approx 1.5 \times 10^{-6}$ of generating two photon pairs from the same source.

Polarization mode manipulation was implemented via PBS and half- and quarter-wave plates (HWP and QWP). Polarization-dependent loss was implemented with a polarizing beam splitter (PBS), rotated around its vertical axis away from the normal incidence condition, accompanied by a HWP for phase and walk-off compensation.

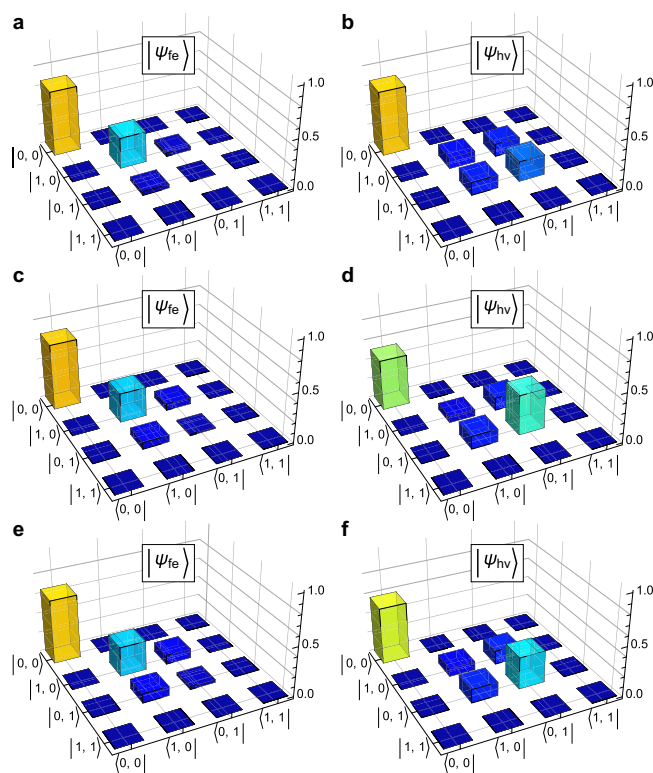


Fig. 4 Absolute values of the density matrix elements for quantum states distributed via different types of channels. **a** Maximally-mode-entangled state sent through an uncorrected quantum channel with $L = 0.988 \pm 0.001$ added loss. **b** Same input state, but distributed through the error-corrected quantum channel with the nominal gain setting from Fig. 3, at which the observed concurrence was the highest. **c, d** and **e, f** same as **a, b**, but with $L = 0.958 \pm 0.001$ and $L = 0.903 \pm 0.002$, respectively.

Data availability

The data that support the plots within this paper and other findings of this study are available in Supplementary Section 1 and from corresponding authors upon reasonable request.

Received: 21 January 2022; Accepted: 11 March 2022;
Published online: 05 April 2022

References

1. Acin, A. et al. Device-independent security of quantum cryptography against collective attacks. *Phys. Rev. Lett.* **98**, 230501 (2007).
2. Flamini, F., Spagnolo, N. & Sciarrino, F. Photonic quantum information processing: a review. *Rep. Prog. Phys.* **82**, 016001 (2019).
3. Slussarenko, S. & Pryde, G. J. Photonic quantum information processing: a concise review. *Appl. Phys. Rev.* **6**, 041303 (2019).
4. Gottesman, D., Jennewein, T. & Croke, S. Longer-baseline telescopes using quantum repeaters. *Phys. Rev. Lett.* **109**, 070503 (2012).
5. Ofek, N. et al. Extending the lifetime of a quantum bit with error correction in superconducting circuits. *Nature* **536**, 441 (2016).
6. Niset, J., Fiurášek, J. & Cerf, N. J. No-go theorem for Gaussian quantum error correction. *Phys. Rev. Lett.* **102**, 120501 (2009).
7. Pan, J.W., Bouwmeester, D., Weinfurter, H. & Zeilinger, A. Experimental entanglement swapping: entangling photons that never interacted. *Phys. Rev. Lett.* **80**, 3891 (1998).
8. Kaltenbaek, R., Prevedel, R., Aspelmeyer, M. & Zeilinger, A. High-fidelity entanglement swapping with fully independent sources. *Phys. Rev. A* **79**, 040302 (2009).
9. Weston, M. M. et al. Heralded quantum steering over a high-loss channel. *Sci. Adv.* **4**, e1701230 (2018).

10. Tsujimoto, Y. et al. Heralded amplification of nonlocality via entanglement swapping. *New J. Phys.* **22**, 023008 (2020).
11. Abdelkhalik, D., Syllwasschy, M., Cerf, N. J., Fiurásek, J. & Schnabel, R. Efficient entanglement distillation without quantum memory. *Nat. Commun.* **7**, 11720 (2016).
12. Chen, L.K. et al. Experimental nested purification for a linear optical quantum repeater. *Nat. Photon.* **11**, 695 (2017).
13. Xu, P. et al. Two-hierarchy entanglement swapping for a linear optical quantum repeater. *Phys. Rev. Lett.* **119**, 170502 (2017).
14. Li, Z.D. et al. Experimental quantum repeater without quantum memory. *Nat. Photon.* **13**, 644 (2019).
15. Xiang, G.Y., Ralph, T. C., Lund, A. P., Walk, N. & Pryde, G. J. Heralded noiseless linear amplification and distillation of entanglement. *Nat. Photon.* **4**, 316 (2010).
16. Ferreyrol, F. et al. Implementation of a nondeterministic optical noiseless amplifier. *Phys. Rev. Lett.* **104**, 123603 (2010).
17. Mićuda, M. et al. Noiseless loss suppression in quantum optical communication. *Phys. Rev. Lett.* **109**, 180503 (2012).
18. Ulanov, A. E. et al. Undoing the effect of loss on quantum entanglement. *Nat. Photon.* **9**, 764 (2015).
19. Meyer-Scott, E. et al. Certifying the presence of a photonic qubit by splitting it in two. *Phys. Rev. Lett.* **116**, 070501 (2016).
20. Kocsis, S., Xiang, G.Y., Ralph, T. C. & Pryde, G. J. Heralded noiseless amplification of a photon polarization qubit. *Nat. Phys.* **9**, 23 (2013).
21. Bruno, N. et al. Heralded amplification of photonic qubits. *Opt. Express* **24**, 125 (2016).
22. Monteiro, F. et al. Heralded amplification of path entangled quantum states. *Quantum Sci. Technol.* **2**, 024008 (2017).
23. Haw, J.Y. et al. Surpassing the no-cloning limit with a heralded hybrid linear amplifier for coherent states. *Nat. Commun.* **7**, 13222 (2016).
24. Ralph, T. C. Quantum error correction of continuous-variable states against gaussian noise. *Phys. Rev. A* **84**, 022339 (2011).
25. Lund, A. P. & Ralph, T. C. Nondeterministic gates for photonic single-rail quantum logic. *Phys. Rev. A* **66**, 032307 (2002).
26. Loredó, J. C. et al. Generation of non-classical light in a photon-number superposition. *Nat. Photon.* **13**, 803 (2019).
27. Caspar, P. et al. Heralded distribution of single-photon path entanglement. *Phys. Rev. Lett.* **125**, 110506 (2020).
28. Minder, M. et al. Experimental quantum key distribution beyond the repeaterless secret key capacity. *Nat. Photon.* **13**, 334 (2019).
29. Drahí, D. et al. Entangled resource for interfacing single- and dual-rail optical qubits. *Quantum* **5**, 416 (2021).
30. Chrzanowski, H. M. et al. Measurement-based noiseless linear amplification for quantum communication. *Nat. Photon.* **8**, 333 (2014).
31. Ralph, T. C. & Lund, A. P. Nondeterministic noiseless linear amplification of quantum systems, in *AIP Conference Proceedings* (ed. Lvovsky, A.), 155 (2009).
32. Pegg, D. T., Phillips, L. S. & Barnett, S. M. Optical state truncation by projection synthesis. *Phys. Rev. Lett.* **81**, 1604 (1998).
33. Chou, C.W. et al. Measurement-induced entanglement for excitation stored in remote atomic ensembles. *Nature* **438**, 828 (2005).
34. Berry, D. W. & Lvovsky, A. I. Preservation of loss in linear-optical processing. *Phys. Rev. A* **84**, 042304 (2011).
35. Weston, M. M. et al. Efficient and pure femtosecond-pulse-length source of polarization-entangled photons. *Opt. Express* **24**, 10869 (2016).
36. Marsili, F. et al. Detecting single infrared photons with 93% system efficiency. *Nat. Photon.* **7**, 210 (2013).
37. Klyshko, D. N. Use of two-photon light for absolute calibration of photoelectric detectors. *Sov. J. Quantum Electron.* **10**, 1112 (1980).
38. Pickston, A. et al. Optimised domain-engineered crystals for pure telecom photon sources. *Opt. Express* **29**, 6991 (2021).

Acknowledgements

This work was conducted by the ARC Centre of Excellence for Quantum Computation and Communication Technology under grant CE170100012. M.M.W. acknowledges financial support through Australian Government Research Training Program Scholarships.

Author contributions

T.C.R. and G.J.P. conceived the idea and supervised the project. S.S. and M.M.W. developed the theoretical model with help from T.C.R., and constructed and carried out the experiment with help from L.K.S., S.K., and G.J.P. V.B.V. and S.-W.N. developed the high-efficiency SNSPDs. All authors discussed the results and contributed to the manuscript. Correspondence and requests for materials should be addressed to S.S., T.C.R., and G.J.P.

Competing interests

The authors declare no competing interests.

Additional information

Supplementary information The online version contains supplementary material available at <https://doi.org/10.1038/s41467-022-29376-4>.

Correspondence and requests for materials should be addressed to Sergei Slussarenko, Timothy C. Ralph or Geoff J. Pryde.

Peer review information *Nature Communications* thanks the anonymous reviewer(s) for their contribution to the peer review of this work.

Reprints and permission information is available at <http://www.nature.com/reprints>

Publisher's note Springer Nature remains neutral with regard to jurisdictional claims in published maps and institutional affiliations.



Open Access This article is licensed under a Creative Commons Attribution 4.0 International License, which permits use, sharing, adaptation, distribution and reproduction in any medium or format, as long as you give appropriate credit to the original author(s) and the source, provide a link to the Creative Commons license, and indicate if changes were made. The images or other third party material in this article are included in the article's Creative Commons license, unless indicated otherwise in a credit line to the material. If material is not included in the article's Creative Commons license and your intended use is not permitted by statutory regulation or exceeds the permitted use, you will need to obtain permission directly from the copyright holder. To view a copy of this license, visit <http://creativecommons.org/licenses/by/4.0/>.

© The Author(s) 2022